Structure of ^{23}F via Beta Decay of ^{23}O

C. S. Sumithrarachchi[1,2],* D. J. Morrissey[1,2], B. A. Brown[1,3], A. D. Davies[1,3], D. A. Davies[1,2], M. Fancina[1], E. Kwan[1,3], P. F. Mantica[1,2], M. Portillo[1], Y. Shimbara[1], J. Stoker[1,2], and R. R. Weerasiri[1,2]
[1]*National Superconducting Cyclotron Laboratory, Michigan State University, East Lansing, MI 48824, USA*
[2]*Department of Chemistry, Michigan State University, East Lansing, MI 48824, USA and*
[3]*Department of Physics and Astronomy, Michigan State University, East Lansing, MI 48824, USA*
(Dated: December 13, 2006)

The nuclear states in ^{23}F have been investigated following the beta decay of ^{23}O. The measurement of ^{23}O was carried out at the NSCL using fragments from the reaction of a ^{48}Ca beam in a Be target. The half-life and the total neutron emission probability were determined to be 97(8) ms and 7(2)%, respectively, for ^{23}O beta decay. Ten gamma-ray decays in ^{23}F and a single gamma-ray in ^{22}F were observed to establish the beta decay scheme for ^{23}O. Shell model calculations are in reasonable agreement with the measured beta branching and B(GT) values for the lowest energy state. The excitation energies of the first $1/2^+$ and $3/2^+$ states have been determined to be 2243(8) and 4066(16) keV, respectively, indicating a widening of the $5/2^+$ - $1/2^+$ state gap in ^{23}F. The decay scheme of the largest contaminant ^{26}Ne in the experiment was established.

PACS numbers: 23.40.-s, 21.60Cs, 23.20Lv, 27.20.+n

I. INTRODUCTION

The disappearance of traditional magic numbers and the appearance of new magic numbers in approaching the drip line are not clearly understood. The study of neutron-rich fluorine isotopes can provide important information on the variation of nuclear shell structure between the doubly magic oxygen isotopes and the island of inversion region in the nuclear landscape. The knowledge of nuclear structure, in particular in ^{23}F, is important as it should be sensitive to the *s* and *d* orbital splitting. ^{23}F also has the structure of a single proton outside the reported doubly magic ^{22}O [1, 2]. The present work focused on the beta-delayed neutrons and gamma-rays from ^{23}O beta decay to establish the energies of neutron bound and unbound states in ^{23}F. This paper presents the study on beta decay of ^{23}O using a neutron spectroscopic array. The results were used to establish the beta decay scheme for ^{23}O that are compared with shell model calculations.

Mueller et al. reported a total neutron emission probability (P_n) of 31(7)% for the beta decay of ^{23}O with a half-life of 82(37) ms, which is the only measurement for the half-life to date [3]. An upper limit for P_n of 29% was subsequently published by Reeder et al. [4]. There is no spectroscopic information for the beta decay of ^{23}O at present, although there are several theoretical estimates of the half-life of ^{23}O that range from 12.8 to 196 ms [3]. All of the predicted P_n values for ^{23}O beta decay were close to 30% and thus agreed with the experimental values with the exception of a value predicted by Wildenthal et al., which was only 2% [5]. The energy levels in the daughter of ^{23}O beta decay were measured using the heavy-ion transfer reaction ^{22}Ne(^{18}O, ^{17}F)^{23}F by Orr et al. [6]. Six energy levels were observed in ^{23}F, in which the ground state, and the second and third excited states were assigned to be spin and parity of $5/2^+$, $7/2^+$ and $9/2^+$, respectively, based on shell model calculations. The ground state in ^{23}F was confirmed to be $5/2^+$ by Sauvan et al. [7]. Two excited states at 3810 and 2900 keV deexcited by a cascade of gamma-rays at 910 and 2900 keV in ^{23}F have been reported by Belleguic et al. [1] using ^{36}S fragmentation reactions with in-beam gamma spectroscopy. These two states were assigned as $7/2^+$ and $9/2^+$, respectively, by comparison to the shell model. Michimasa et al. recently reported studies of the excited states in ^{23}F using three kinds of reactions, namely ^{4}He(^{22}O, ^{23}Fγ), ^{4}He(^{23}F, ^{23}Fγ) and ^{4}He(^{24}F, ^{23}Fγ) [8]. The gamma-ray decay scheme was established up to 7 MeV based on gamma-gamma coincidence measurements. The energy levels at 2268(12) and 4059(11) keV were tentatively assigned to be $1/2^+$ and $3/2^+$, respectively. The spins and parities for other states are unknown and no negative parity states in ^{23}F have been observed at present. The ground state of ^{23}O is known to be $1/2^+$ [7] so that we expect beta feeding predominately to excited states as direct feeding to the ground state would be a first forbidden decay.

II. EXPERIMENTAL

The experiment was carried out at the National Superconducting Cyclotron Laboratory of Michigan State University. The radioactive beam of ^{23}O was produced by projectile fragmentation of a 140 MeV/nucleon ^{48}Ca beam in a 846 mg/cm^2 thick Be target placed at the object position of the A1900 fragment separator. The fragments were separated by the A1900 separator using a combination of two magnetic bends (magnetic rigidities: 4.497 and 4.210 Tm) along with a 825 mg/cm^2 Al wedge placed at the middle image position of the A1900, and a relatively narrow momentum acceptance ($\Delta p/p =$

*Electronic address: chandana@nscl.msu.edu

TABLE I: The beam purity of ^{23}O experiment from the A1900 and in the implantation detector

Nuclide	A1900 Purity[a](%)[b]	Implantation Detector Purity[c](%)	Literature half-life[d] (ms)
^{23}O	16.8	14.2	82(37)
^{26}Ne	62.2	83.1	192(6)
^{24}F	7.4	2.1	400(50)
^{21}N	1.5	0.6	85(7)

[a]At the A1900 focal plane from the TOF and energy loss measurement.
[b]^{25}F, ^{27}Ne, ^{10,11,12,13}Be, ^{7,8,9}Li and ^{6}He contribute to the remaining 12.1%.
[c]Taken from the difference in counts of silicon detectors.
[d]Taken from Ref. [10].

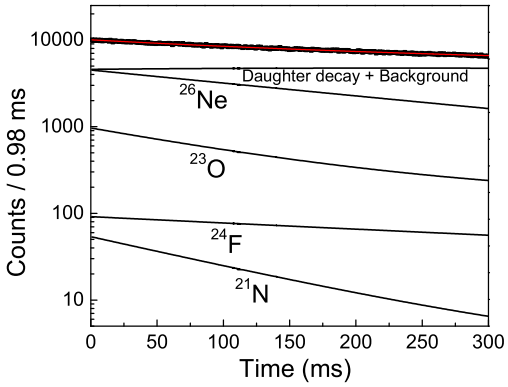

FIG. 1: The beta decay curve of ^{23}O. The total fit to the decay curve, the individual decay components of the implanted ^{26}Ne, ^{23}O, ^{24}F and ^{21}N, and the background plus all decay contributions of daughters and granddaughters decay are shown.

TABLE II: Detected beta decay events from ^{23}O experiment

Nuclide	Total number of beta decay events	Half-life (ms)
^{23}O	$1.47(4)\times10^5$	102(23)[a]
^{26}Ne	$8.61(2)\times10^5$	192(4)[b]
^{24}F	$2.21(7)\times10^4$	384(16)[b]
^{21}N	$6.53(5)\times10^3$	85(14)[c]

[a]By fitting the decay curve, see the text.
[b]Gamma-ray gated half-lives from present work.
[c]Taken from Ref. [14].

0.5%). A detailed description of the device and method is given in Ref. [9]. The secondary beam was a cocktail beam consisting of ^{23}O, ^{26}Ne, ^{24}F and ^{21}N with fractions given in Table I. In addition, ^{16}C and ^{17}N radioactive beams used to calibrate the neutron spectroscopic array were produced separately by changing the magnetic rigidities of the A1900 using the same target and wedge.

The decay data were measured in a beam-on/off batch mode. The beam was pulsed on for a period of 300 ms to collect nuclides in the implantation detector and the beta decay was monitored during a beam-off period of 300 ms. The beam-on/off period was selected based on the half-life value of ^{23}O in the literature [3]. The experimental station consisted of an implantation detector, an array of sixteen neutron time-of-flight (TOF) detectors and eight gamma-ray detectors. The fragments passed into air through a kapton window, followed by a silicon detector and an aluminum degrader before reaching the implantation detector. The implantation detector (3 mm plastic scintillator) produced a start signal for the neutron and gamma-ray detectors at the detection of a beta decay event during the beam-off period. On-line particle identification was performed based on the time-of-flight from the production target and energy loss information from the silicon detectors. A second silicon detector was placed approximately 8 cm after the implantation detector to monitor particles that punched through. An aluminum degrader was placed before the implantation detector and adjusted to a thickness of 11.412 mm so that ^{23}O was fully stopped in the implantation detector. The information from both silicon detectors was used to determine the composition of the implanted beam given in Table I.

Sixteen neutron detectors were used to measure beta-delayed neutrons from ^{23}O beta decay. The detectors were curved with a radius of 1 m to get an equal flight path for neutrons from the implantation detector, which was located at the center of the array. The details of the design of the neutron bar array and the calibration procedures for energy and efficiency can be found in Ref. [11, 12]. The neutron detection efficiency function was defined by well-known beta-delayed neutrons from ^{16}C and ^{17}N, and three Monte Carlo calculated data points. The total neutron efficiency was found to be 2.26% at 1.0 MeV.

Beta-delayed gamma-rays were detected using eight detectors from the Segmented Germanium Array (SeGA) [13]. The detectors were placed in a ring structure where the detector crystals were parallel to the beam at a radius of 14 cm and 19.2 cm away from the implantation detector. The SeGA detectors were calibrated using off-line sources of ^{60}Co, ^{207}Bi and ^{152}Eu, and the well-known gamma-rays from the daughters of the impurities. The total gamma-ray efficiency of the SeGA detectors was measured to be 1.9% at 1 MeV.

III. RESULTS

A. Total number of beta decay events

The total number of beta decay events detected by the implantation detector was determined by fitting the beta decay curve with a function that contains contributions from the decays of all implanted nuclides and their de-

cay chains. The model was written for each implanted decay series using Bateman equations [15] and included the growth of each nuclide during the beam-on period. The nuclides that did not decay during the beam-off period were added to the next cycle. The implantation purity ratios, taken from the measurement of silicon detectors, were used to fix the relative initial activities of the implanted isotopes. The half-lives of all daughters and granddaughters, and the half-life of ^{21}N, which are reported in the literature [10], have been kept as constants through the fitting procedure. The half-lives of ^{26}Ne and ^{24}F, which were deduced from the gamma-ray gated decay curves (see below) were also added to the model as fixed values. In addition, the neutron emission probabilities of ^{24}F and ^{21}N were included by using the values of 5.9% and 81%, respectively, as reported in the literature [10]. Four parameters were left as variables: the half-life of ^{23}O, the implantation rate of ^{26}Ne, the neutron emission probability of ^{23}O and a constant background. The individual contributions to the decay from each implanted nuclide are shown in Fig. 1 with the total daughter and granddaughter contributions plus the background. The number of beta decay events extracted by integrating the individual components are given in Table II with the half-life and their uncertainties from different sources given. The half-life values and the P_n value of ^{23}O were found to be 102(23) ms and 11(9)% by the fitting, respectively. The large number of activities present in the detector does not allow precise measurement of the half-lives in the bulk activity.

B. Neutron and gamma-ray measurement

The total neutron time-of-flight spectrum measured during the beam-off period and corrected for the constant-fraction discriminator (CFD) walk in all of the detectors in the neutron spectroscopic array is shown in Fig. 2. The position of the beta-gamma prompt peak provides the time zero reference point for the time-of-flight spectrum. Cosmic rays predominately propagate in the opposite direction through the detection system and trigger the electronics at shorter time relative to the betas to produce the cosmic-ray peak in Fig. 2. No neutron peaks can be observed within the detection limits. The lower and upper detection limits are approximately 360 and 8000 keV, respectively. Since the energy window that is available for beta decay into the neutron unbound states is limited to 3750 keV (channel number 112), the energies of neutrons are within the upper detection limit. It is possible that low energy beta-delayed neutrons from beta decay of ^{23}O were below the lower energy detection limit of the neutron bar array and a search for the gamma-rays that originated from the beta-delayed neutron daughter decay was undertaken.

Fig. 3 shows the gamma-ray spectrum obtained in coincidence with the beta decay of the ^{23}O cocktail during the beam-off period. The peaks are labeled with their

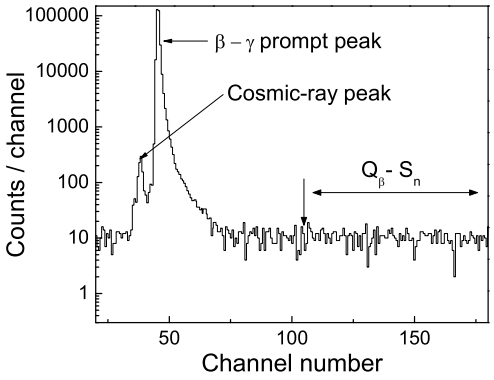

FIG. 2: Beta-delayed neutron time-of-flight spectrum of ^{23}O obtained by adding all neutron detectors in the array. The peak due to cosmic-ray interaction with neutron detectors and the beta-gamma prompt peak are shown. The upper limit of the beta decay energy window to the neutron unbound states is indicated.

parent nucleus and energy in keV. The beta decay of ^{23}O leads the mass (A) = 23 decay chain yielding the decays of ^{23}F and ^{23}Ne. The gamma-ray transitions at 493, 816, 1017, 1701, 1822, 1920, 2132, 2316, 2415, 2734, 3432 and 3831 keV were identified from the beta decay of ^{23}F based on the previous ^{23}F beta decay measurements [14]. The assignments were reconfirmed by determining the gated half-lives for peaks that were statistically significant. Two gamma-rays from ^{23}Ne beta decay, the granddaughter of ^{23}O, were observed at 440 and 1637 keV with the emission probabilities of 33.0 and 1.1%, respectively. These observations were also in good agreement with the literature values [14]. The gamma-ray transitions from the decay of the impurities in the cocktail beam, such as ^{26}Ne, ^{24}F and ^{21}N, and their daughters and granddaughters are shown and labeled in Fig. 3. The gamma-ray transitions associated with the A = 26 decay chain will be addressed separately below. In addition, a gamma ray at 1980 keV was identified from the beta decay of ^{24}F, which was also reported in Ref. [14]. The gated half-life of 384(16) ms confirms the assignment. A few gamma-rays from the A = 21 decay chain determined in previous experiments are also labeled in Fig. 3.

Although beta-delayed neutrons from ^{23}O beta decay were not observed, gamma-ray peaks associated with the beta decay of ^{22}F, the beta-delayed neutron daughter of ^{23}O were observed at 1274, 2083 and 2166 keV. These weak transitions had an intensity ratio of 5:4:3. This observation leads to the conclusion that at least one of the ^{22}F states is populated by beta-delayed neutron decay of ^{23}O since nuclides with A = 22 were not implanted. Excited states in ^{22}F were studied previously in beta decay of ^{22}O [16], and ^{22}Ne(^{3}He, t) and ^{22}Ne(^{7}Li, ^{7}Be) reactions [17]. A weak gamma-ray at 638 keV was observed that is consistent with neutron feeding of the 3^+

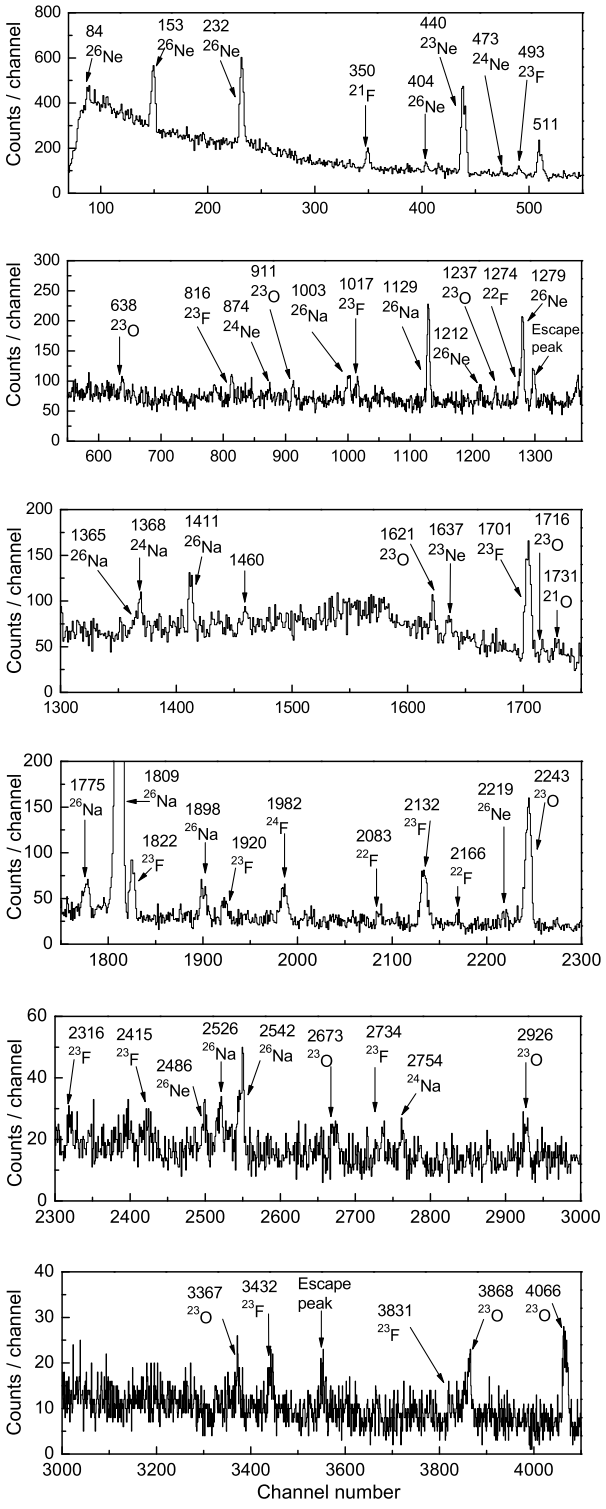

FIG. 3: The beta-gamma coincidence spectrum of the implanted nuclei. The gamma-ray peak energies are given in keV with their beta decay assignments.

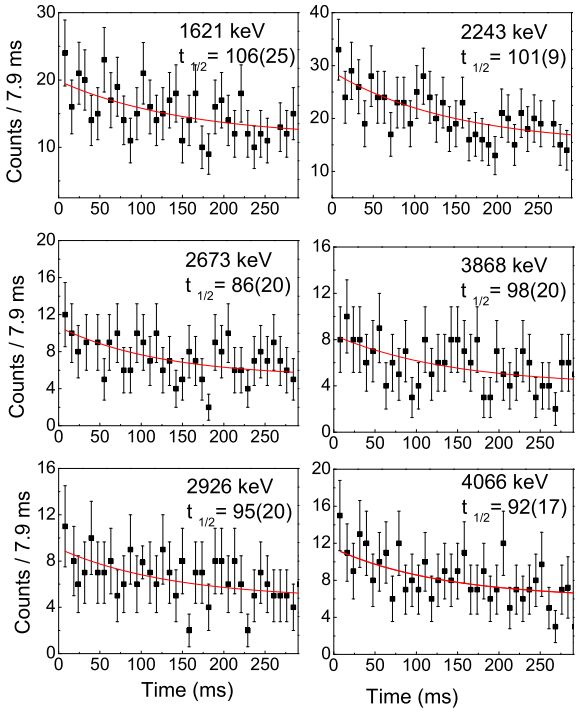

FIG. 4: The gamma-ray gated decay curves. The fitted single exponents are shown for the statistically significant peaks corresponding to beta decay of ^{23}O. The gated gamma-ray peak energies and corresponding gated half-lives are given in keV and ms, respectively.

state. The gamma-ray at 72 keV in cascade with the 638 keV transition was not seen due to the threshold of SeGA detectors. Thus, although the neutrons were not observed as discussed above, the observation of the A = 22 decay chain and a weak transition in ^{22}F indicate a total beta-delayed neutron emission probability at the level of 7(2)%, which was calculated by considering the total beta decay of ^{22}F derived from the observed gamma-ray activities in ^{22}Ne. Note that the parent and daughter activities in this decay series were saturated during the 30-minute long runs.

The relatively strong gamma-ray transitions of 1621, 2243, 2673, 2926, 3868 and 4026 keV were identified from the beta decay of ^{23}O, which agree with previous work [1, 8]. The gated half-lives were obtained by fitting a single exponential plus background to the gated decay curves, shown in Fig. 4. The deduced gated half-lives are shown in the figure and are labeled by gamma-ray energy. The weighted average of the gated half-lives was 97(8) ms. Although the half-life of ^{21}Na is 85(7) ms, the above gamma-ray transitions can not be attributed to the ^{21}Na beta decay since the number of implanted nuclides were not enough to produce such strong peaks. Four gamma-rays at 912, 1237, 1716 and 3367 keV were also attributed to ^{23}O beta decay based on the work of

Belleguic et al. and Michimasa et al. [1, 8]. The gamma-ray at 912 keV was in good agreement with both previous measurements. The transitions at 1237, 1716 and 3367 keV also matched within uncertainties with the reported transitions in Ref. [8]. Gamma-ray peaks at 2003, 3445, 3985 and 4732 keV reported in the nuclear reaction study were not observed in the present work.

C. ^{26}Ne analysis

The largest implanted contaminant, ^{26}Ne, decays to ^{26}Na, which subsequently decays to the stable nucleus ^{26}Mg. This nucleus was recently studied by Weissman et al. and we will only briefly report our confirmation of this work with new shell model calculations. Eight gamma-rays associated with the daughter of ^{26}Ne beta decay known from the literature [14] were observed and they were labeled in Fig. 3 by their energy and the parent nuclide. With the exception of the 2219 keV gamma-ray, the other transitions in Table III were attributed to the beta decay of ^{26}Ne based on a recent beta decay experiment [18]. The gated decay curves were generated for transitions that were statistically significant and the half-lives determined in the above mentioned procedure are given in Table III. The weighted average of the half-life was found to be 192(4) ms, which is in good agreement with previous work [18]. In addition, a weak gamma-ray at 2219(4) keV was found which could be the gamma-ray transition at 2232(15) keV in ^{26}Na observed in nuclear reaction studies by Lee et al. [19]. The gamma-ray at 1996 keV [19] reported in the same work was not seen although both gamma-rays were reported to deexcite the same energy level. The emission probability of the 84 keV gamma-ray was not determined due to high threshold of some of the SeGA detectors, thus this value was adopted from Ref. [18] and used in beta branch calculations. The level scheme for beta decay of ^{26}Ne, shown in Fig. 5(A), has been constructed from the experimental observations. There was no beta decay feeding to the ground state of ^{26}Na as the number of ^{26}Na beta decay events deduced from gamma-ray activities was in good agreement with the number of gamma-ray cascading events to the ^{26}Na ground state.

New shell model calculations for the beta decay of ^{26}Ne and ^{26}Na were performed in *sd*-shell model space using the recent USDB interaction [20]. Fig. 5(B) shows the ^{26}Ne beta decay scheme constructed from the shell model calculations. Beta decay branches and the gamma-ray emission probabilities higher than 0.1% are shown. The comparison of both decay schemes shows reasonable agreement between our data and the shell model calculations. However, Lee et al. have argued that older shell model calculations clearly disagree below 3 MeV with the experimental results of the beta decay of ^{26}Ne from the work of Weissman et al. based on the nonobservation of a 1^+ state in ^{26}Na predicted to have a relatively strong beta branch [19]. They also supported their argument by providing a similar situation in the beta decay of ^{28}Ne. Our results show the missing 1^+ state could be the state at 2219 keV. The level ordering obtained by new shell model calculations supports this assignment although the beta feeding does not match as well.

TABLE III: Gamma-ray assignment for beta decay of ^{26}Ne

Gamma energy(keV)	Gated half-life(ms)	Emission Probability(%)	Nuclide	Level (keV)
84(3)	-	95[a]	^{26}Na	84
153(3)	192(4)	3.4(2)	^{26}Na	234
232(2)	193(4)	4.4(2)	^{26}Na	234
404(3)	-	0.4(1)	^{26}Na	404
1212(3)	190(10)	1.2(3)	^{26}Na	2723
1279(3)	-	5.4(2)	^{26}Na	1513
2219(4)	-	0.6(2)	^{26}Na	2219
2486(4)	-	0.7(2)	^{26}Na	2723

[a]From Ref. [18]

TABLE IV: Gamma-ray assignment for beta decay of ^{23}O

Gamma energy(keV)	Gated half-life(ms)	Emission Probability(%)	Nuclide	Level (keV)
911(4)	-	2.7(12)	^{23}F	3837
1237(4)	-	3.1(9)	^{23}F	4604
1621(6)	106(25)	5.7(10)	^{23}F	3866
1716(6)	-	2.1(6)	^{23}F	5553
2243(8)	101(9)	51.5(12)	^{23}F	2243
2673(9)	86(20)	5.2(10)	^{23}F	5599
2926(10)	95(20)	7.2(18)	^{23}F	2926
3367(13)	-	4.5(10)	^{23}F	3367
3868(15)	98(20)	10.1(16)	^{23}F	3866
4066(16)	92(17)	17.1(17)	^{23}F	4066
638(3)	-	1.5(8)	^{22}F	710

D. Beta decay scheme of ^{23}O

The assignments of gamma-rays to the energy levels in ^{23}F were based on known energy levels and corresponding gamma-ray transitions observed in previous experiments, since beta-delayed gamma-gamma coincidence events were not observed due to poor statistics. The gamma-ray transition at 638 keV deexcites the energy level at 710 keV in the neutron daughter ^{22}F following Ref. [17]. The gamma-ray transitions of 2243, 2926, 3367, 3868 and 4066 keV were assigned to feed the ground state of ^{23}F as reported in Ref. [8]. The gamma-rays of 912, 1237 and 2673 keV were placed depopulating the known states at 3837, 4604 and 5599 keV, respectively, to be consistent with the gamma decay scheme in ^{23}F as given in Ref. [8]. The 3837 keV state was fed by the gamma-ray of 1716 keV originated from the known state at 5553 keV. This tentative placement is reasonable because it matches with the difference in known energy levels and the intensity flow. Although the gamma-ray

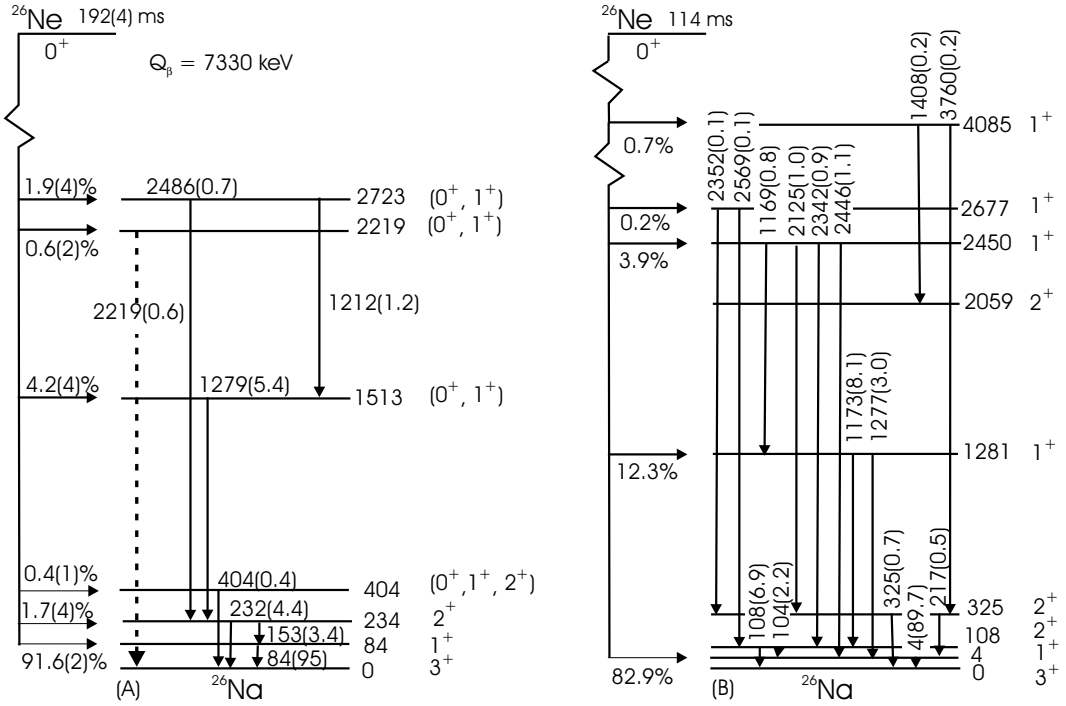

FIG. 5: The experimental decay scheme for ^{26}Ne (A): The gamma-ray decay is given in vertical arrows with the transition energy and emission probabilities in parenthesis. The horizontal arrow shows the beta decay feeding to the level with the beta branch and the corresponding uncertainty in parenthesis. The dashed arrow shows a new gamma-ray transition. The experimental weighted average half-life is given. The theoretical decay scheme (B): The decay scheme is constructed with a minimum limit of 0.1% for the beta branch and gamma emission probability. The notation for the gamma-ray decay is explained as above and the beta branch is given on the horizontal arrow. The calculated half-life is 114 ms.

at 1621 keV was not seen in previous experiments, this could be assigned to the 3866 keV state based on the energy difference between the known energy levels at 2243 and 3866 keV. Table IV shows the observed gamma-rays with their uncertainties, the gated half-lives, the gamma emission probabilities and the energy level assignments for the beta decay of ^{23}O.

The proposed beta decay scheme of ^{23}O, shown in Fig. 6(A), is based on the known energy levels in ^{23}F and the observed energy and intensity sum rules. The absolute beta decay branching to each populated level was calculated by taking the difference between gamma-ray decay into and out of the level, normalized to the total decay. The branching is shown on horizontal arrows in Fig. 6(A) with uncertainties in parenthesis. The gamma-ray energies and their emission probabilities in parenthesis are given on the vertical arrows. The gamma-ray feeding to the ground state and the total ^{23}F beta decay events calculated from the gamma-rays associated with ^{23}F decay were consistent within uncertainties. This leaves negligible beta decay feeding to the ground state. The beta decay branches were not calculated for the states at 2926, 3367 and 3837 keV since the feeding and deexcitation intensities agreed within uncertainties. The observation of the 638 keV gamma-ray suggested that beta-delayed neutrons could feed the excited state in ^{22}F as shown in Fig. 6(A). The neutron bound states associated with very small beta decay feeding and weak gamma-ray decay could be existed as the beta decay window of 2 MeV is opened inbetween the highest observed energy state from the present work and the neutron separation energy. The apparent log(ft) values were calculated for the observed states in ^{23}F using the method in Ref. [21] with the measured half-life, the beta decay branch (given in Table V) and the Q_β value from Ref. [17]. Table V shows the calculated beta decay branches, log(ft) values and Gamow-Teller transition strengths (B(GT)) for the observed bound states along with their spin and parity assignments. B(GT) values were calculated according to Ref. [22] using the log(ft) values.

Six allowed beta decays with the spin and parity assignments of $1/2^+$ or $3/2^+$ are reasonable from the measured log(ft) values and the selection rules of beta decay considering the ^{23}O ground state has a $1/2^+$. The states at 2243 and 4066 keV were given spin and parity assignments of $1/2^+$ and $3/2^+$, respectively, to be consistent with the corresponding assignments given by Michimasa et al. [8].

Shell model calculations for the beta decay of ^{23}O were performed using a USDB interaction and free-nucleon Gamow-Teller operator for beta allowed decay. The predictions were done in *sd*-shell model space with considering a $1/2^+$ ground state for ^{23}O. Fig. 6(B) shows the beta

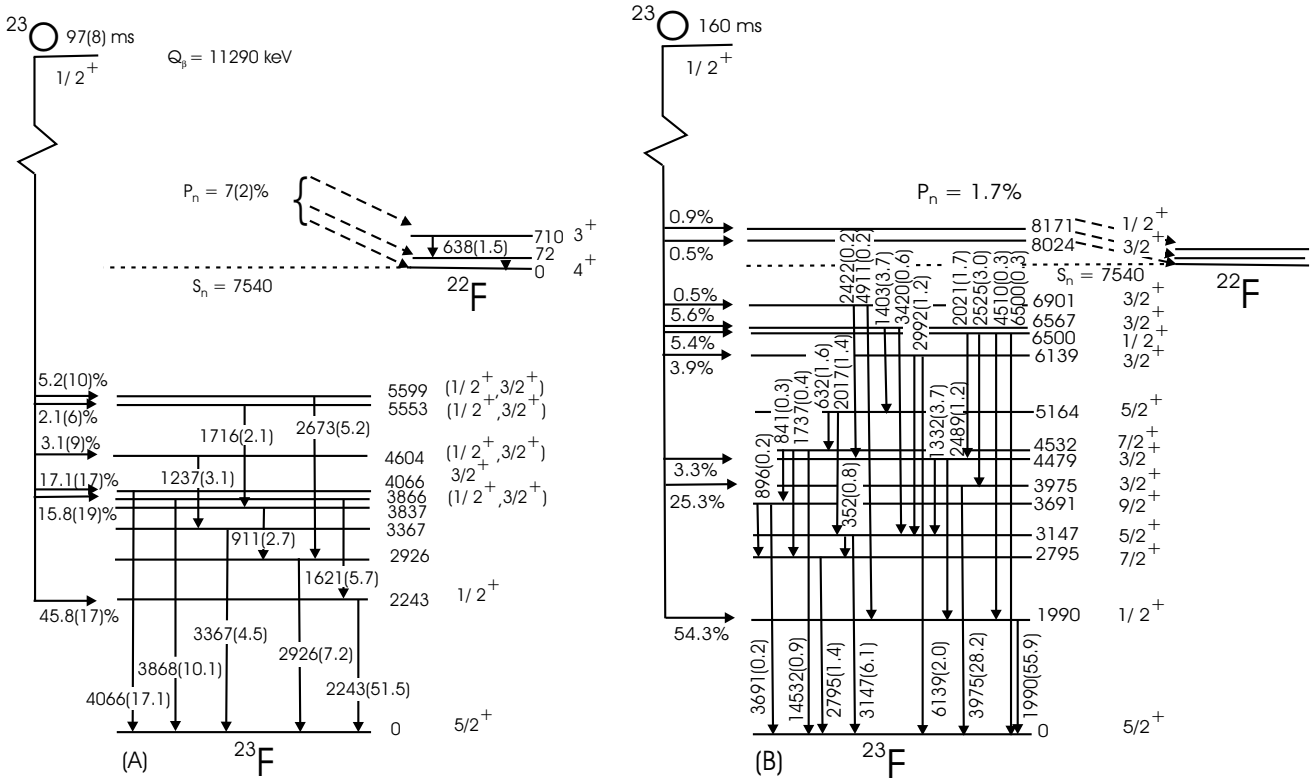

FIG. 6: The beta decay scheme of ^{23}O. (A) The experimental decay scheme: The gamma-ray decay was given in vertical arrows with the transition energy and emission probabilities in parenthesis. The horizontal arrow shows the beta decay feeding to the level with the beta branch and the corresponding uncertainty in parenthesis. The weighted average half-life and P_n value from this experiment, and Q_β value from Ref. [17] are given on the top of scheme. (B) The theoretical decay scheme: The gamma-ray emission probabilities and branches higher than 0.2% are shown with the calculated half-life.

decay scheme for ^{23}O with gamma-ray decays and beta branches greater than 0.2% deduced from shell model calculations. Our calculations predict nine states that are fed by the allowed beta decays with branches greater than 0.2%, and in which two states are above the single neutron separation energy leading to neutron decay. The calculations indicate major branches of 54.3 and 25.3% to the states at 1990 ($J^\pi = 1/2^+$) and 3975 keV ($J^\pi = 3/2^+$), respectively. The total neutron emission probability was predicted to be 1.7% with a half-life of 160 ms as shown in Fig. 6(B). In addition, gamma-ray decay in ^{23}F, shown in Fig. 6(B), was calculated in the same model space to produce the deexcitation scheme. The overall agreement between the two decay schemes is reasonable within the detection limits.

TABLE V: The properties of ^{23}O beta decay.

Energy level (keV)	Branch (%)	Log(ft)	Spin parity	B(GT)
2243	45.8(17)	4.27	$1/2^+$	0.32
2926	0	-	-	-
3367	0	-	-	-
3837	0	-	-	-
3866	15.8(19)	4.33	$(1/2^+, 3/2^+)$	0.29
4066	17.1(17)	4.24	$3/2^+$	0.36
4604	3.1(9)	4.82	$(1/2^+, 3/2^+)$	0.09
5553	2.1(6)	4.68	$(1/2^+, 3/2^+)$	0.13
5599	5.2(10)	4.28	$(1/2^+, 3/2^+)$	0.32

IV. DISCUSSION

The weighted half-life of 97(8) ms for beta decay of ^{23}O measured in this experiment is consistent with the half-life reported by Mueller et al. [3] and it is not in good agreement with our predicted value of 160 ms. The half-life obtained with the USDB interaction for the neighboring ^{22}O beta decay of 1.4 s is shorter than the experimental value of 2.3(1) s [16]. The ^{22}O half-life shows the typical hindrance of experiment relative to theory for Gamow-Teller decay in the *sd*-shell [23]. A similar hindrance is also observed for the ^{26}Ne decay. In contrast, the experimental decay for ^{23}O half-life of 97(8) ms is enhanced relative to theory. The reason for this enhancement is not understood. The total neutron emission probability of 7(2)% from present work is inconsistent with the experimental values in the literature and also with most of theoretical predictions except for that

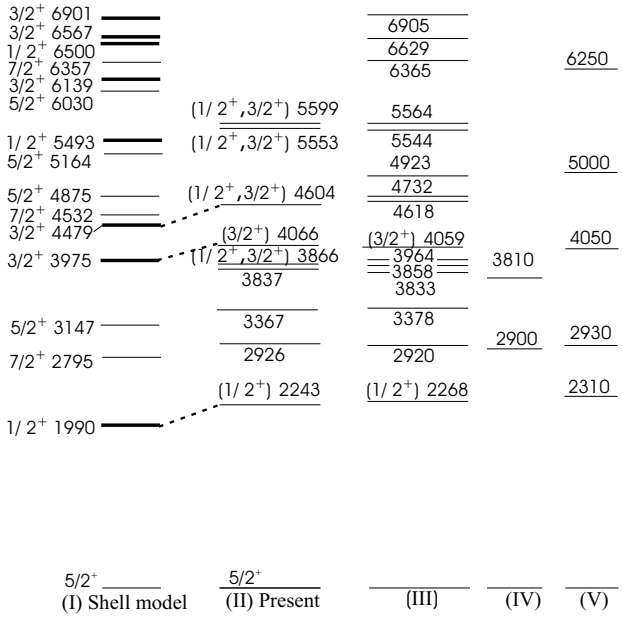

FIG. 7: ^{23}F levels from the present experiment along with present shell model calculations and previous works. Shell model predicted (I) allowed beta decay states in thick lines and forbidden beta decay states in thin lines, and the energy levels from the present work (II) and work of Michimasa et al. (III), Belleguic et al. (IV) and Orr et al. (V) are shown. The likely calculated and experimental states are combined with the dotted lines. All energies are given in keV.

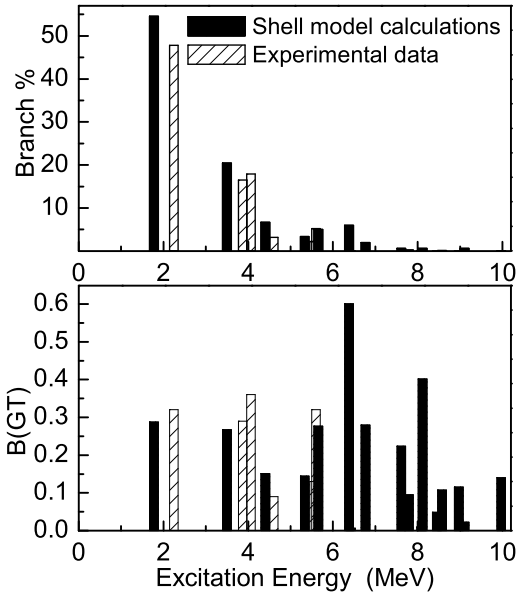

FIG. 8: The comparison of beta decay branching (top) and Gamow-Teller strengths (bottom) between shell model predictions and the experiment values for the beta decay of ^{23}O.

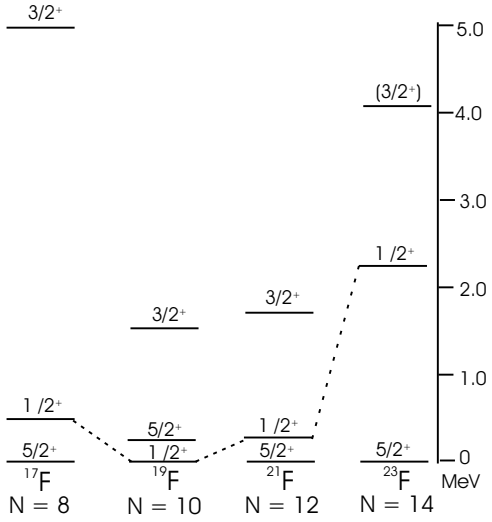

FIG. 9: The location of experimental energy states in odd-mass fluorine isotopes as a function of neutron number.

of Wildenthal et al. [5] and our new calculations using USDB interactions of about 2%. The neutron branch was observed by the gamma-rays associated with the daughter ^{22}F and no neutrons were observed with energy above approximately 360 keV.

The level scheme for ^{23}F from the present work can be compared in Fig. 7 with our shell model calculations in *sd*-shell model space and previous experimental work. The first $1/2^+$ state located at 2243 keV is about 253 keV higher than the shell model predicted state at 1990 keV. The level at 4066(16) keV was assigned to be $3/2^+$ in the previous work by Michimasa et al. on the basis of spectroscopic factors. Our new shell model calculations also indicate that the state at 3975 keV [24] contains about 50% of the total $d_{3/2}$ spectroscopic strength, thus the calculated 3975 keV state was associated with the observed level at 4066 keV. The next higher shell model state with the spin and parity of $3/2^+$ at 4479 keV should be associated with the 4604 keV state. Noting that there are no other low spin states in the calculations near 3.8 MeV and the apparently low spectroscopic factor for the 3858(11) keV state in the work of Michimasa et al., the state observed at 3866(13) keV in this experiment cannot be associated any of states obtained in the *sd* model space. It could be an intruder state with its observation in beta decay due to a strong mixing with the *sd*-shell states. The thick lines in Fig. 7 show the predicted beta decay levels in ^{23}F that have beta decay branches greater than 0.2%. The experimental beta decay branching and B(GT) values are compared with the corresponding predicted values in Fig. 8. The experimental values for beta decay branching and B(GT) for the first $1/2^+$ state agree reasonably with the shell model predictions. The beta decay feeding to the states at 3866 keV and above is not consistent with the calculations. The inconsistency is highlighted by the difference of the B(GT) values.

Fig. 9 shows the variation of the energies of the low-

est $5/2^+$, $1/2^+$ and $3/2^+$ states in odd-mass fluorine isotopes. The ground states of fluorine isotopes have a single proton in the proton $d_{5/2}$ orbital and fill neutrons into the neutron $d_{5/2}$ orbital as the mass of the isotope increases. The comparison of experimental energy gaps in the fluorine isotopes shows a sudden increase in the gap between $5/2^+$ and $1/2^+$ states in ^{23}F as shown in Fig. 9. This could be an indication of the appearance of N = 14 shell closure in this region.

V. SUMMARY

The present work reports the first spectroscopic decay study of ^{23}O finding a half-life of 97(8) ms and a total neutron emission probability of 7(2)%. Six allowed beta decay transitions were observed including three strong decays to the states at 2243, 3866 and 4066 keV. The comparison of shell model calculations of the beta decay showed a reasonable agreement for energies below 4604 keV. The analysis of energy states in fluorine isotopes suggests a widening in the $1/2^+$ and $5/2^+$ energy gap in ^{23}F.

Acknowledgments

We would like to thank the staff of the NSCL for their assistance during experiments. This work was supported by the National Science Foundation under grants PHY-01-10253 and PHY-0555366 .

[1] M. Belleguic, M. J. Lpez-Jimnez, M. Stanoiu, F. Azaiez, M. G. Saint-Laurent, O. Sorlin, N. L. Achouri, J. C. Anglique, C. Bourgeois, C. Borcea, et al., Nucl. Phys. A **682**, 136c (2001).
[2] P. G. Thirolf, Phys. Lett. B **485**, 16 (2000).
[3] A. C. Mueller, D. Guillemaud-Mueller, J. C. Jacmart, E. Kashy, F. Pougheon, A. Richard, A. Staudt, H. V. Klapdor-Kleingrothaus, M. Lewitowicz, R. Anne, et al., Nucl. Phys. A **513**, 1 (1990).
[4] P. L. Reeder, R. A. Warner, W. K. Hensley, D. J. Vieira, and J. M. Wouters, Phys. Rev. C **44**, 1435 (1991).
[5] B. H. Wildenthal, M. S. Curtin, and B. A. Brown, Phys. Rev. C **28**, 1343 (1983).
[6] N. A. Orr, L. K. Fifield, W. N. Catford, and C. L. Woods, Nucl. Phys. A **491**, 457 (1989).
[7] E. Sauvan, F. Carstoiu, N. A. Orr, J. C. Anglique, W. N. Catford, N. M. Clarke, M. M. Cormick, N. Curtis, M. Freer, S. Grvy, et al., Phys. Lett B **491**, 1 (2000).
[8] S. Michimasa, S. Shimoura, H. Iwasaki, M. Tamaki, S. Ota, N. Aoi, H. Baba, N. Iwasa, S. Kanno, S. Kubono, et al., Phys. Lett B **638**, 146 (2006).
[9] D. J. Morrissey, B. M. Sherrill, M. Steiner, A. Stolz, and I. Wiedenhoever, Nucl. Instrum. Methods Phys. Res. A **204**, 90 (2003).
[10] www.nndc.bnl.gov/ensd/.
[11] R. Harkewicz, D. J. Morrissey, B. A. Brown, J. A. Nolen, N. A. Orr, B. M. Sherrill, J. S. Winfield, and J. A. Winger, Phys. Rev. C **44**, 2365 (1991).
[12] C. S. Sumithrarachchi, D. W. Anthony, P. A. Lofy, and D. J. Morrissey, Phys. Rev. C **74**, 024322 (2006).
[13] W. F. Mueller, J. A. Church, T. Glasmacher, D. Gutknecht, G. Hackman, P. G. Hansen, Z. Hu, K. L. Miller, and P. Quirin, Nucl. Instrum. Methods Phys. Res. A **466**, 492 (2001).
[14] P. M. Endt, Nucl. Phys. A **521**, 1 (1990).
[15] H. Bateman, Proc. Cambridge Philos. Soc. **15**, 423 (1910).
[16] L. Weissman, A. F. Lisetskiy, O. Arndt, U. Bergmann, B. A. Brown, J. Cederkall, I. Dillmann, O. Hallmann, L. Fraile, S. Franchoo, et al., J. Phys.G **31**, 553 (2005).
[17] R. B. Firestone, Nucl. Data Sheet **106**, 1 (2005).
[18] L. Weissman, O. Arndt, U. Bergmann, J. Cederkall, I. Dillmann, O. Hallmann, L. Fraile, S. Franchoo, L. Gaudefroy, U. Koster, et al., Phys. Rev. C **70**, 057306 (2004).
[19] S. Lee, S. L. Tabor, T. Baldwin, D. B. Campbell, I. Calderin, C. Chandler, M. W. Cooper, C. R. Hoffman, K. W. Kemper, J. Pavan, et al., Phys. Rev. C **73**, 044321 (2006).
[20] B. A. Brown and W. A. Richter, Phys. Rev. C **74**, 034315 (2006).
[21] N. B. Gove and M. J. Martin, Nucl. Data Tables **10**, 205 (1971).
[22] K. W. Scheller, J. Gorres, S. Vouzoukas, M. Wiescher, B. Pfeiffer, K. L. Kratz, D. J. Morrissey, B. M. Sherrill, M. Steiner, M. Hellstrom, et al., Nucl. Phys. A **582**, 109 (1995).
[23] B. A. Brown and B. H. Wildenthal, Atomic dat. and Nucl. dat. Tab. **33**, 347 (1985).
[24] A. Signoracci and B. A. Brown, Phy. Rev. C to be published.